Spin Hall effect tip for scanning tunneling microscopy experiments on quantum materials

THESIS

submitted in partial fulfillment of the
requirements for the degree of

MASTER OF SCIENCE
in
PHYSICS

Author :	K.M. Bastiaans
Student ID :	0947962
Supervisor :	Dr. M.P. Allan
2^{nd} corrector :	Prof. Dr. Ir. T.H. Oosterkamp

Leiden, The Netherlands, July 28, 2015

Spin Hall effect tip for scanning tunneling microscopy experiments on quantum materials

K.M. Bastiaans

Huygens-Kamerlingh Onnes Laboratory, Leiden University
P.O. Box 9500, 2300 RA Leiden, The Netherlands

July 28, 2015

Abstract

Many of the physical phenomena observed in quantum materials exhibit interesting magnetic order. Resolving their spin structure with atomic-scale resolution provides an insight in the microscopic physics involved. We believe that a device-based method for spin polarized STM will enable the needed control and reliability to resolve the spin structure in many of the quantum materials. In this thesis we present the spin Hall effect tip as a potential candidate. It will employ the spin Hall effect to generate a pure spin polarized tip driven by an electrical current. By making a distinction between the intrinsic and extrinsic spin Hall effect, and reviewing their different characteristics, we argue that a copper host doped with bismuth impurities (CuBi) is the most promising material for fabricating spin Hall effect based devices. Testing of a CuBi spin Hall bar yet need to be carried out to investigate the feasibility of implementing a spin Hall effect device on a STM tip. The first steps towards this device are presented in this report.

Contents

Chapter 1

Motivation

The world of the quantum materials is a breeding place of fascinating and interesting new physics. During the past decades it already revealed some of its mysteries, leading to the discovery of several new states of matter; for instance the high T_c superconductors, heavy fermion systems, topological insulators and other mysterious states in the vicinity of the quantum critical point.

Being able to probe these new states of matter locally is crucial for exploring the quantum materials and to gain a microscopic understanding of their underlying new phenomena. Scanning tunnelling microscopy (STM) proves to be a powerful technique to explore the quantum materials [1–3], because it is able to visualize the surface with atomic-scale resolution and also resolve its electronic structure. For instance the electronic structure of cuprate superconductors [1], Cooper pairing in a heavy fermion system [2] and nematic structure in iron based superconductors [3] are already explored by the use of STM. Since many of these phenomena also exhibit interesting magnetic order, it would be of great interest to be able to resolve also the spin structure with atomic-scale resolution. This would provide a way to obtain a more microscopic understanding of the magnetic ordering in many quantum materials.

The concept of spin polarized STM (SP-STM) is not new [4]; by creating a well defined spin polarization on the tip, only electrons with a certain polarization are available for tunneling. Under the assumption that these spins don't flip while tunneling, the tunneling current then strongly dependents on the spin polarization of the local density of states on the sample. This enables SP-STM to resolve the relative polarization of the

spins on the sample. Two main techniques are common for polarizing the tip, namely using a ferromagnetic tip or coating the apex of the tip with a small cluster of magnetic atoms. [4–6] Unfortunately both techniques seem to lack the control and reliability to resolve the spin structure in quantum materials. Mainly because an external magnet is needed to focus or switch the polarization of spins on the tip.

We believe that a device-based method would provide the needed control and reliability. In this thesis we will discuss a new tool (illustrated in figure 1.1), a potential candidate for resolving the spin structure of quantum materials: the spin Hall effect tip. The structure of this thesis is the following: the background theory on the spin Hall effect will be reviewed in chapter 2, in chapter 3 we will discuss a method to verify the presence of the spin Hall effect and chapter 4 we will propose how to unite the spin Hall effect on a STM tip and discuss its potential application for spin polarized STM.

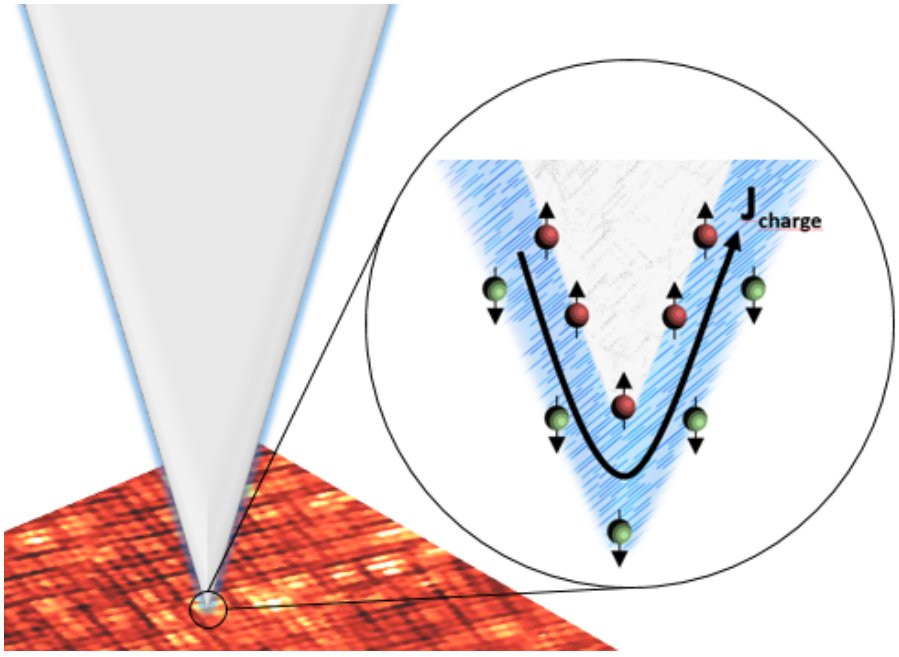

Figure 1.1: *The idea for the Spin Hall Effect tip; a device based tip for SP-STM to resolve the spin structure in many quantum materials (like the 'checkerboard' state in the lightly doped cuprate superconductor $Ca_{2-x}Na_xCuO_2Cl_2$ [7] in this figure). The insulating tip is coated with a thin layer of material (blue) that exhibits the spin hall effect. By applying a charge current through this thin layer, a spin imbalance is generated, polarizing the tip. The polarization can be switched by changing the direction of the current.*

Chapter 2

Spin Hall Effect

First predicted by D'yakonov and Perel in 1971 [8], and later independently revived by Hirsch (1999) [9] and Zhang (2000) [10], surprisingly a charge current propagating through a paramagnetic metal, in the absence of an external magnetic field, can generate a transverse spin imbalance. Hirsch christened this the "Spin Hall Effect" due to the strong similarities to the anomalous Hall effect. In this chapter we will discuss the relevant background theory, followed by the first experimental evidence confirming conversion from charge to spin current. We will then make a distinction between an "intrinsic" and "extrinsic" origin of the effect and, based on this background theory, argue which material is best suited for a spin Hall effect device.

2.1 Background Theory

The spin Hall effect describes the conversion from a charge to a spin current in a nonmagnetic metal. The basic picture is illustrated in figure 2.1 Consider a nonmagnetic metal, with no external magnetic field applied, carrying a charge current (j_x in the $+x$ direction in figure 2.1). Electrons, carrying a spin, will scatter in a direction perpendicular to the charge current due to "internal" or "external" scattering mechanisms. This happens in a way that electrons carrying spin up will scatter in the opposite direction of electrons carrying spin down. What these mechanisms are we will discuss later, for now we will just stick to this basic picture. Since the total number of electrons with spin up and spin down is equal, the splitting wont generate a charge imbalance. This means there will not be a bias voltage perpendicular to the charge current. But there will be more

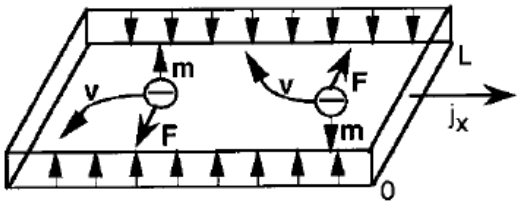

Figure 2.1: *Basic picture of the spin Hall effect by Hirsch [9]. Spin up and down electrons split in opposite direction, transverse to the direction of the charge current.*

spins pointing up on one side and more spins down on the opposite side (as illustrated in the figure). Hence what happens is that there will be a spin imbalance generated perpendicular to the charge current. In this way the spin Hall effect converts a charge current into a perpendicular spin current. Usually this is expressed as

$$j_{spin} = \Theta_{SH}(\sigma \times j_{charge}) \tag{2.1}$$

where j_{spin} is the generated transverse spin current, σ the spin of the electron and j_{charge} the charge current. A figure of merit for this electronics to spintronics conversion is the so-called spin Hall angle Θ_{SH}, it expresses the conversion yield between spin and charge current.

Now the question becomes what scattering mechanism drives the spin splitting. We will distinguish two flavors of spin Hall effect with a different origin, the ”intrinsic” and the ”extrinsic” type.

2.1.1 Intrinsic scattering

The mechanism of intrinsic scattering was first described by Sinova *et al.* (2004). [11] Systems that show a purely intrinsic spin hall effect are characterized by a strong Rashba spin-orbit coupling. Here the spin-orbit coupling causes the spins to align perpendicular to the momenta, recall the Rashba spin-orbit coupling Hamiltonian

$$H = \frac{p^2}{2m} - \frac{\lambda}{\hbar}\vec{\sigma} \cdot (\vec{z} \times \vec{p}) \tag{2.2}$$

where λ is the Rashba coupling constant, $\vec{\sigma}$ the spin of the electron, $\vec{p}$ the angular momentum and $\vec{z}$ a unit vector perpendicular to the momenta plane. This alignment in momentum space due to the Rashba spin-orbit

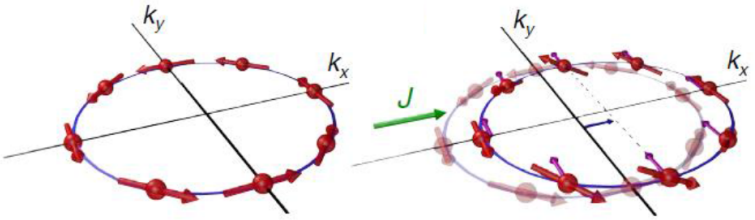

Figure 2.2: *Illustration by Sinova et al. to describe the intrinsic spin Hall effect due to strong Rashba spin-orbit coupling. [12] Spins align perpendicular to momentum according to the Rashba Hamiltonian (2.2). When an electric field is applied, the Fermi surface moves through momentum space, tilting the spins, which results in a spin current perpendicular to the electric field.*

coupling is also illustrated in figure 2.2.

When an electric field is applied ($+x$ direction in figure 2.2), the electrons are accelerated and the Fermi surface moves along in the direction of the electric field. Due to the movement in momentum space the electrons feel an additional spin-orbit field. As a reaction spins in the $+y$ direction tilt up and spins in the $-y$ direction tilt down, resulting in a spin current in the y direction (perpendicular to the electric field). [12] In this way the intrinsic spin-orbit coupling generates a spin imbalance that is perpendicular to the applied electric field.

2.1.2 Extrinsic scattering

The other type of scattering that leads to the spin Hall effect is of an "external" origin. It is found in compounds of noble metals doped with strong spin-orbit coupled impurities, where anisotropic scattering by impurities leads to a separation of spin up and down.

Two mechanisms, both related to the strong spin-orbit coupling of the impurities, can contribute to the extrinsic spin Hall effect [13]; skew scattering [14] and scattering with side jumps [15]. Both are illustrated in figure 2.3.

When an electric field is applied, electrons are accelerated along the direction of the field. These electrons scatter anisotropically on the doping impurities due to the strong spin-orbit coupling. As said, this can happen in two ways. Either by skew scattering (figure 2.3 a.), this is characterized by having different possibilities for electrons to scatter in different direc-

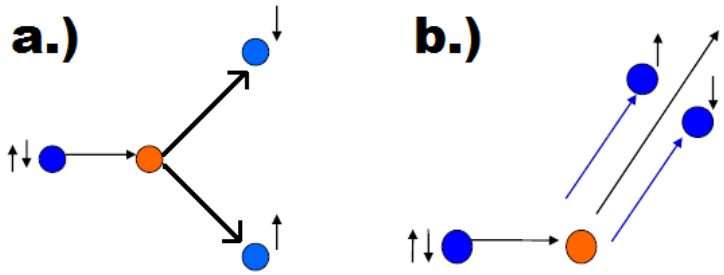

Figure 2.3: *Anisotropic scattering by impurities, two kinds of mechanism. a.) Skew scattering. Spin up and down scatter in opposite direction. b.) Scattering with side jumps. When scattering, spin up and down make a side jump in opposite direction.*

tions. Electrons carrying a spin of opposite sign will scatter in opposite direction. [16] Or scattering with side jumps occurs (figure 2.3 b.). When deflecting of an impurity, spin up and down make a side jump in opposite direction. [17] Both mechanisms result in a separation of spins up and down, perpendicular to the direction of the charge current.

2.2 Experiment and Materials

After the principles of the spin Hall effect were proposed by by Hirsch (1999) and Zhang (2000) [9, 10], the first experimental proof followed in 2006. Valenzuela and Tinkham were the first to measure the conversion of an injected spin current to a (measurable) charge current in aluminium, hereby verifying the existence of the spin Hall effect. [18]

The problem that they had to overcome was how to measure the spin current electronically. Valenzuela and Tinkham anticipated on the idea that if a charge current induces a transverse spin current through spin-orbit interaction, the opposite will also hold due to the symmetry of the relation. Injecting a spin current will induce a transverse charge imbalance.

Their experiment, that verified the spin Hall effect concepts, is shown in figure 2.4. By injecting a spin current using two ferromagnetic contacts, a voltage was measured in the transverse direction over the aluminium strip. This confirmed that the spin Hall effect can effectively generate spin polarized currents, or can be used to directly measure them.

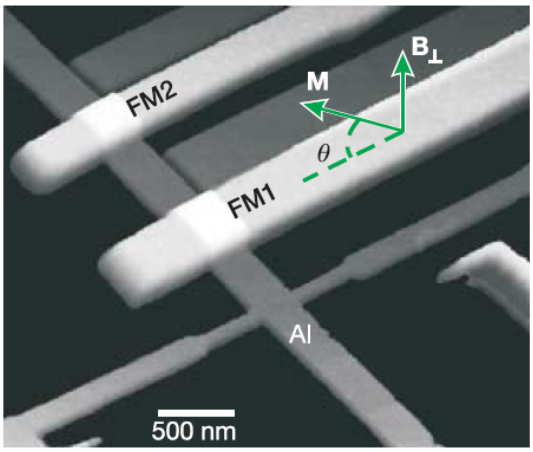

Figure 2.4: *Aluminium hall bar configuration with two ferromagnetic contact to inject a spin current. Valenzuela and Tinkham used this structure to verify the existence of the spin Hall effect. [18]*

2.2.1 Length scales: the spin diffusion length

Following on this, the spin Hall effect was also showed to be present in the strong spin-orbit coupled platinum, using the same technique as Valenzuela and Thinkham. [19] Next were tantalum [20] and tungsten [21], but now investigated by spin torque switching experiments. However, the fact that this all concerned strong spin-orbit coupled materials turns out to be a limitation for practical application. If one would like to make use of the generated spin imbalance and maintain a pure spin current, the imbalance would have to persist over the whole length scale of the device. The characteristic distance over which a single spin can move before flipping its spin is the spin diffusion length l_s. [22] Typically this length is short for strong spin-orbit coupled metals (in the order of a few nm). This turns out to be the limiting factor for fabricating pure spin current devices made of intrinsic spin hall effect materials.

To both get the strong conversion from charge to spin current and have it polarized over a practical length, the extrinsic spin hall effect is more promising. [23, 24] Gradhand *et al.* (2010) made this prediction from *ab initio* calculations in the search for the best materials to use in pure spin current devices. The merger of a noble metal doped with few strong spin-orbit coupled impurities should combine best of both worlds. The light host (such as copper or gold) makes that the spin diffusion length is long, the heavy impurities act as the scattering sides responsible for the spin

splitting. Calculations show that a conversion yields of approximately 10% combined with a spin diffusion lengths of 100 nm are feasible. [23, 25]

2.2.2 Extrinsic spin hall alloys

CuIr
A great advantage of doping a noble metal with impurities is that the strength of the extrinsic spin hall effect can be tailored by choosing the right combination of host and impurity metal. A conversion yield of $2.1 \pm 0.6\%$ is reported for iridium doped copper (CuIr), measuring a spin diffusion length of roughly 30 nm. [26] This value of the spin diffusion length already exceeds that of pure platinum by a factor of 10, which exhibits a similar spin hall angle. [19, 27]

AuW / AuPt
An even higher spin hall angle of 10% is reported for a gold host doped with tungsten impurities (AuW). [28] However, since a relative large amount of W impurities are needed to obtain the large conversion yield, the spin diffusion length is reduced to only 2 nm. Doping the gold host with platinum impurities (AuPt) results in a comparable conversion of 12%, over a length of 10 nm. [29]

CuBi
The most interesting alloy is bismuth doped copper (CuBi), reporting a spin hall conversions yield of 24% and a spin diffusion length of roughly 80 nm. [30, 31] At the moment this seems to be the most promising material for spin hall effect based devices, due to its efficient generation of charge into spin current, combined with the relatively long spin diffusion length. New methods are already proposed to even further optimize the composition and dimensions of CuBi based devices. It is predicted that conversion yields of 80% should be possible. [32]

For our purposes it is important that the generated spin current persists over the total length scale of the device. The relatively large spin diffusion length combined with the large spin Hall angle reported for CuBi motivates us to use this material for device fabrication. In the next chapter we will discuss a CuBi structure that we have developed to explore the possibilities of this material for generating spin polarized currents in spin Hall effect devices.

Chapter 3

Spin Hall Bar

Since spin hall effect experiments and devices are rather new concepts (the first successful experiments are only a few years ago), assembling a spin hall device on a STM tip would be a great step forward in both the field of spin hall effect based devices as for spin polarized STM. The total number of successful spin hall experiments is still small and is mostly limited to a few research groups in the world. As a consequence there are no established methods yet for spin hall device fabrication. Therefore we will first make dedicated structures, before fabricating the spin hall tip, in order to verify that the spin hall effect is present in our devices. These structures, called Hall bars, will have the shape of an H. They are inspired on the structures used in the experiment of Brüne *et al.* (2010) who were the first to electronically measure the spin hall effect directly without injecting a spin current. [33]

3.1 Design of spin Hall bar

3.1.1 Structure

We will make H shaped structures to verify that the spin hall effect is present in the material and methods we will use for our device. The concept of the H structure is the following (also illustrated in figure 3.1): a charge current is applied through one of the standing legs of the Hall bar (left leg in figure 3.1), in the presence of the spin Hall effect this generates a transverse spin current (through the bridging part of the H). This spin current converts again through the other leg of the H (right leg in figure 3.1) in a measurable charge current. Thus by applying a charge cur-

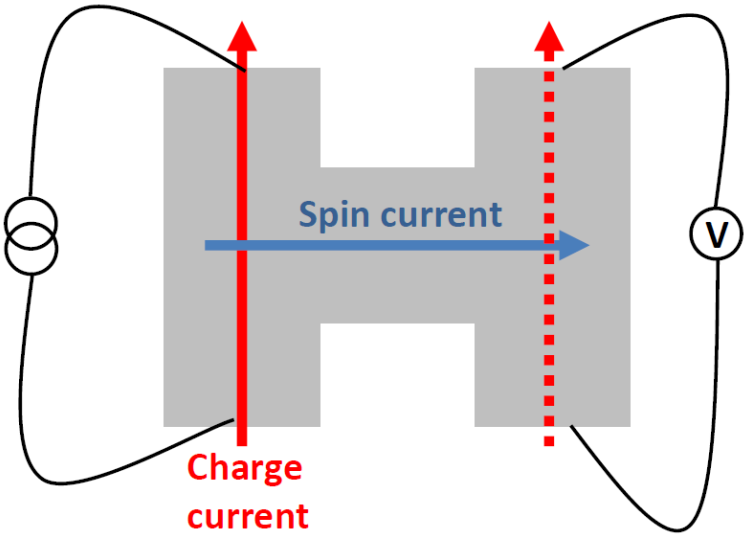

Figure 3.1: *The so-called spin Hall bar, an H shaped structure for non-local detection of the spin Hall effect. A charge current is applied through the left leg, which generates a perpendicular spin current, this is converted again to a charge current through the right leg.*

rent through one of the legs a charge current in the other leg is indirectly induces, thanks to the spin Hall effect. Therefore the presence of the spin Hall effect can directly be detected by measuring the voltage over the leg opposite to the one a charge current is applied through.

3.1.2 Dimensions

Crucial for this non-local detection of the spin Hall effect is the dimension of this H shaped structure. Since the polarized spins diffuse through the material and generate an electrical current elsewhere, the range over which these spins can diffuse before flipping spin (the spin diffusion length l_s) is important. Also the mean free path of the electrons plays a role here. One should choose the dimensions of the structure such that the signal generated by the diffusing spin current can be distinguished from Ohmic transport. To determine the exact geometry and dimensions of the Hall bar we will have to consider the magnitude of both the electric signal generated by the spin Hall effect and the Ohmic behavior.

3.1.3 Spin Hall resistance

Abanin *et al.* (2009) calculated the non-local electric response in the spin Hall bar, focusing on the extrinsic spin Hall effect. [34] According to this calculations, the non-local voltage (generated in the presence of the spin Hall effect) in this H bar geometry equals:

$$\delta V = \frac{\Theta_{SH}^2 \rho w}{2 l_s} I \exp -L/l_s \tag{3.1}$$

where Θ_{SH} is the spin Hall angle (equation 2.1), ρ is the resistivity, w is the width of the bridging channel, l_s is the spin diffusion length, I the current through the opposite leg and L the length of the bridging channel. This description of the non-local voltage is accurate as long as the width w of the bridging section is larger than the electron mean free path. Since in the extrinsic spin hall effect regime we deal with metallic hosts, the electron mean free path is smaller than the dimensions of the device. [31]

3.1.4 Ohmic resistance

The Ohmic behavior is set by the geometry of the H structure. The magnitude of the Ohmic resistance for this geometry is described by the theory of van der Pauw [34, 35]:

$$R_{ohm} = R_{sq} \exp -\frac{\pi L}{w} \tag{3.2}$$

where $R_{sq} = \rho/t$ is the sheet resistance of the H structure having resistivity ρ and thickness t, L is again the length of the bridging part and w the width. The voltage due to the Ohmis transport can thus be described by $\delta V = IR_{ohm} = IR_{sq} \exp -\frac{\pi L}{w}$, with I the applied charge current.

3.1.5 Design of CuBi Hall bar

The H shaped structures are made of CuBi, since this alloy provides the best combination of large spin Hall angle ($\Theta_{SH} = 0.24$) and long spin diffusion length ($l_s = 86$ nm). [30, 31] Considering equations 3.1 and 3.2, we are able to calculate the optimal dimensions of the Hall bar. This to reach the regime where the signal due to the spin Hall resistance can be distinguished from the Ohmic transport. We anticipate on a 20 nm film thickness, equal to the structures in the reports of Niimi *et al.* [30, 31], and the resistivity of CuBi to be similar to that of ordinary Cu; $\rho = 3.2 \mu\Omega cm$

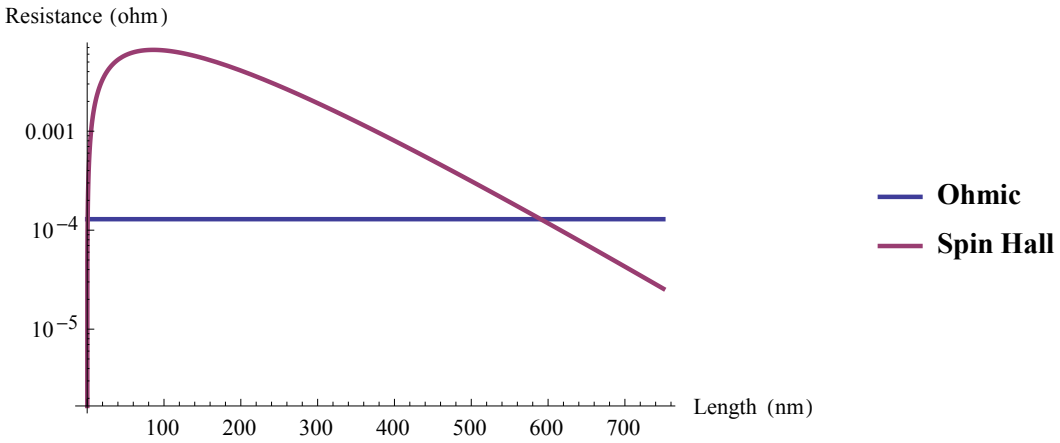

Figure 3.2: *Semi-log plot of calculated spin Hall and Ohmic resistance for different lengths of the CuBi spin Hall bar (equations 3.1 and 3.2).*

(this can be rationalized since the amount of impurities dopants in CuBi is only 0.5%).

Figure 3.2 shows the calculated resistances for both to the spin Hall and Ohmic transport (equations 3.1 and 3.2). Here the typical geometry of a Hall bar is considered of $L = 3w$. Clearly the spin Hall signal can be distinguished from Ohmic transport, as long as the dimensions of the structure are in the range of $L = 50$ to 400 nm. At $L = 600$ nm the spin Hall signal becomes smaller than the Ohmic transport. This calculation sets a regime for the dimensions of the CuBi Hall bar.

3.2 Fabrication

In this section we will discuss the fabrication of the CuBi spin Hall bars, which will consist of three steps: 1. patterning 2. deposition and 3. interfacing. A general overview of the procedure is depicted in figure 3.3.

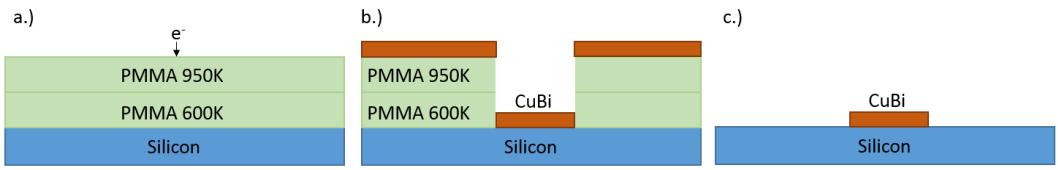

Figure 3.3: *a.) Patterning b.) depostion and c.) lift-off, ready to interface.*

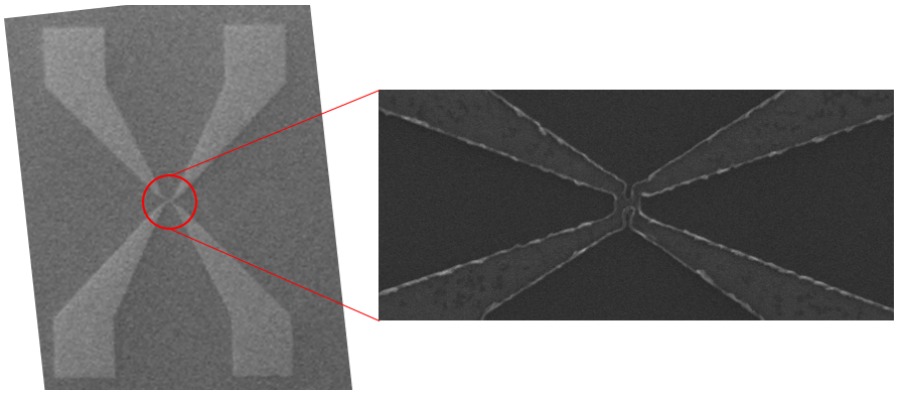

Figure 3.4: *General overview of the Hall bar structure. Left a SEM image of the total structure; four contact pads are connected via narrowing legs to the H shaped structure, shown on the right.*

3.2.1 Patterning

In the previous section we determined that the dimensions of the CuBi Hall bar should be in the range of $L = 50$ to 400 nm. This is a regime that can be accessed with electron beam (e-beam) lithography, using an electron beam patterning generator (EBPG). A high purity, low resistive, *n*-doped silicon wafer with a native oxide layer is cleaned by sonicating it in a acetone, ethanol and isopropanol (IPA) bath. After sonicating the wafer is heated to 150°C for 1 minute on a hotplate, to evaporate all the leftover solvents. Then a double layer of PMMA e-beam lithography resists is spin-coated on the wafer. First a 450 nm thick PMMA 600K layer, baked for 3 minutes on a 150°C hotplate, followed by a 200 nm thick PMMA 950K layer, again baked for 3 minutes on a 150°C hotplate.

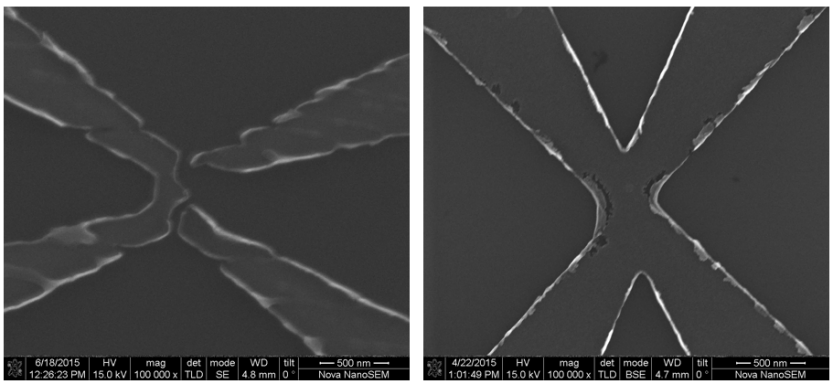

Figure 3.5: *Dose is important. Left: too low dose. Right: too high dose.*

A Raith 100 EBPG is used to pattern the H shaped structure in the double layer of PMMA; spot size 35 nm and an area dose of $285 \mu C/cm^2$. These are important parameters, and strongly depent on what wafer and resist are used. Examples of a too low or high dose is shown in figure 3.5. After patterning the resist is developed for 60 seconds in MIBK:IPA (1:3), and stopped for 60 seconds in IPA.

3.2.2 CuBi deposition

After patterning of the structure, the CuBi material is deposited. This is done by DC magnetron sputtering (Leybold LH Z400), using a Bi sintered Cu target with 0.5% Bi concentration. The sputter deposition was performed in an Ar gas flow of 5E-3 mbar and a 1kV DC potential. Due to the low melting temperature of Bismuth (270°C), the sample shouldn't be heated above 90°C while and after deposition, therefore the wafer is cooled during sputtering. [30]

The remaining resist is lift-off by sonicating for a few seconds in acetone, leaving only the CuBi Hall bar structure remaining on the silicon wafer. Figure 3.6 shows SEM image of the crucial part of the CuBi H-structure after lift-off.

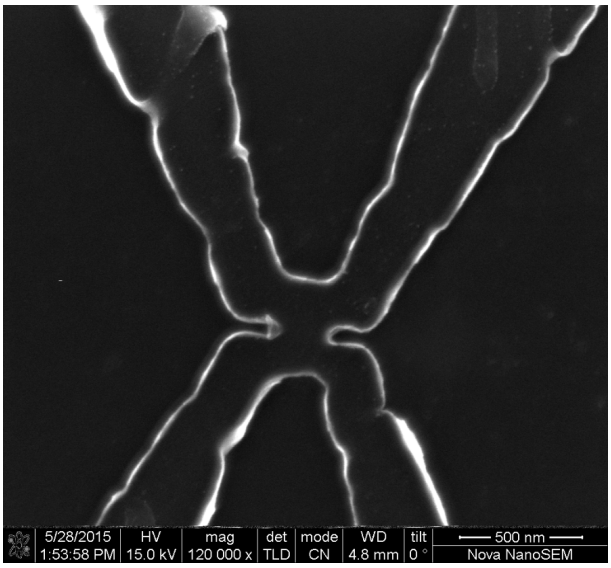

Figure 3.6: *SEM image of a CuBi Hall bar structure. One can identify the two legs connected by a bridging section (the H shape from figure 3.1)*

3.3 Interfacing the CuBi structure

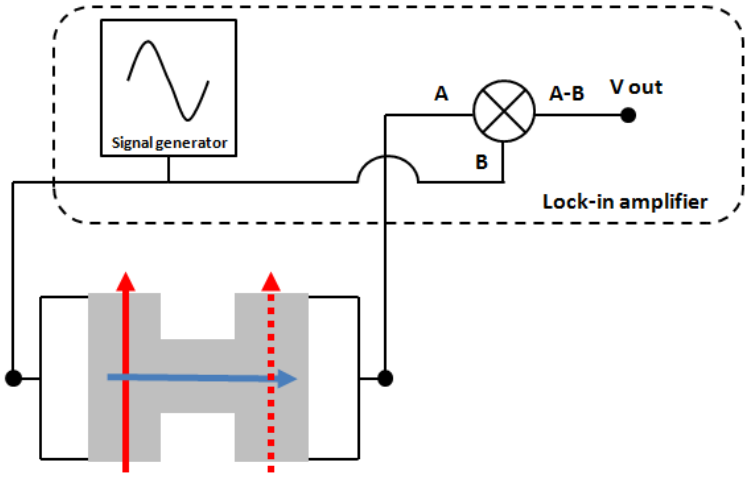

Figure 3.7: *Simplified representation of the 4-point lock-in measurement technique to measure the spin Hall voltage. Additional filters and amplifiers present in the lock-in amplifier are left out for convenience. The arrows in the H shaped structure correspond to description in figure 3.1*

To measure the spin Hall voltage that is associated with the spin Hall effect we propose the 4-point lock-in measurement technique (figure 3.7). A lock-in measurement at $f = 30$ kHz should provide a better signal to noise ratio compared to DC measurements. There are no indications that such low frequent alternating currents change the behavior of the spin Hall effect. The principle is similar the an ordinary 4-point measurement, except the current is now applied through one leg of the Hall bar and the voltage is measured over the other leg. In the presence of the spin Hall effect the applied current converts to a perpendicular spin current, that subsequently translates to a measurable voltage over the opposite leg (as described in section 3.1 and equation 3.1).

At the moment of writing we just entered the measurement phase. Testing of the CuBi spin Hall bar yet need to be performed to investigate the generation of a pure spin polarized current is these Hall bar structures.

Chapter 4

Spin Hall Tip & Outlook

4.1 Spin Hall tip

The final goal of this spin Hall effect tip project is to make a spin polarized STM tip that has the control and reliability to resolve the spin structure in many quantum materials. In this section we will propose our ideas to approach this. The method we propose is inspired by the scanning SQUIDs on a tip, where a insulating tip is covered from two sides with a superconducting layer of material that connects at the apex of the tip, forming two parallel Josephson junctions. [36–39]

It all starts with an insulating tip, quartz or borosilicate glass, with an outer diameter of 1.0 mm. These tips are pulled from rods using a micropipette puller (the concept of micropipette pulling is illustrated in figure 4.1). The rod is heated in the middle and being pulled on from both sides. Once the rods breaks, using the right pulling force and time, two nice sharp tips are formed. The apex diameter of the tip can controllably varied down to $\sim$ 100 nm. [36]

After pulling the insulating tip, it is coated from two sides with a thin layer of CuBi, forming a connection only at the point of the tip. This is done in two steps of DC magnetron sputtering (illustrated in figure 4.2). In the first step one side of the tip is covered by a 20 nm thick CuBi layer. Then the tip is rotated and during a second step it is coated on the other side, leaving a gap between the two layers. Both layers will connect at the apex, resulting in a thin layer of CuBi going around the pointy glass tip.

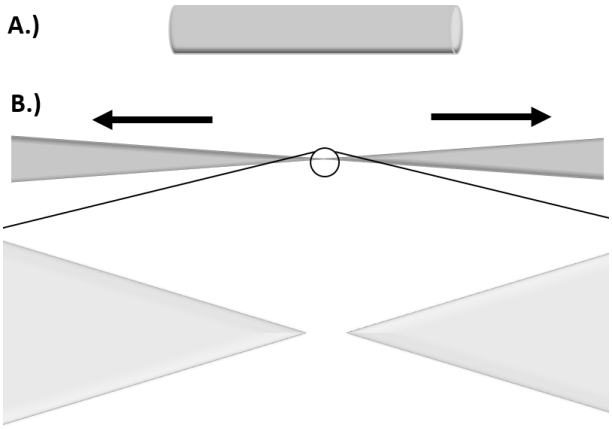

Figure 4.1: *Micropipette pulling; under the right conditions a quartz or borosilicate glass rod (A.) is pulled to break into two nicely sharp tips (B.).*

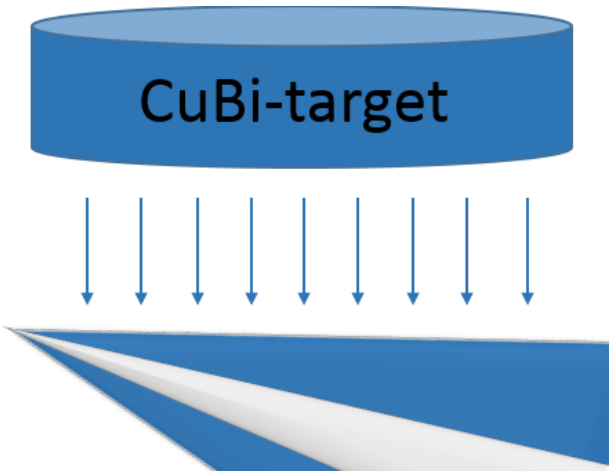

Figure 4.2: *CuBi coating the insulating tip by DC magnetron sputtering. The CuBi coated parts are indicated in blue, on top is the CuBi sputtering target.*

As reviewed in chapter 2, a copper host doped with bismuth impurities is a promising candidate for spintronics devices, since it exhibits a large extrinsic spin Hall effect. When applying a charge current through the thin layer of CuBi coated on the tip, a spin imbalance will be generated, spin polarizing the in- and outside of the CuBi layer, and thereby spin polarizing the tip (figure 4.3). The net polarization of spins on the tip can be tuned by the direction of the applied current. This implies full electrical control of the spin polarization of the tip.

4.2 Outlook

We opened the route towards a spin Hall effect tip. CuBi appears to be to most promising material to use as a coating for the insulating tip. Further investigation of the CuBi Hall bar structures will provide more insight in spin Hall device fabrication. Measuring the generation of a pure spin current in CuBi using the H shaped structures will enable us to take the step forward towards assembling the spin Hall tip.

Imagine one could use such a spin Hall tip for spin polarized STM. It would profit from its easy and quick control of the spin polarization. By applying a current through the coating of the tip, the apex polarizes and only polarized electrons are available for tunneling. The spin Hall tip will also profit from its device-based nature, providing more control and robustness concerning fabrication compared to the spin polarized STM alternatives. It will also add the opportunity to implement additional functionalities to the tip, by the means of nano-fabrication. Eventually the spin Hall tip will enable researchers to investigate the interesting magnetic order and spin structure present in many quantum materials, and by doing so obtain a microscopic understanding of the underlying physics.

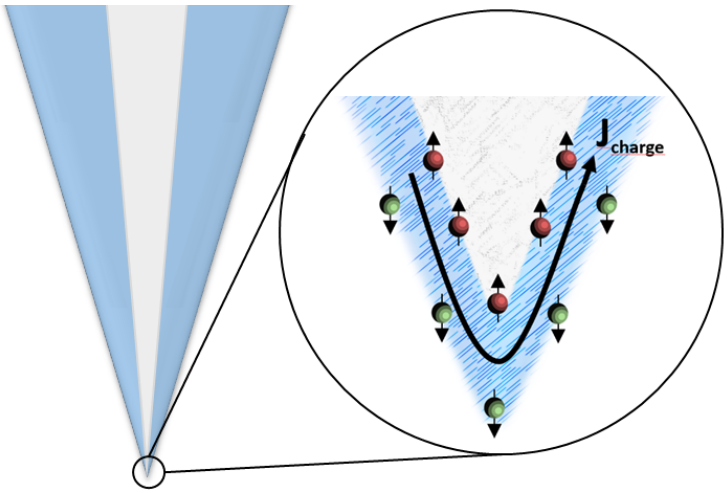

Figure 4.3: *The spin Hall effect tip. An insulating tip (borosilicate glass, indicated in grey) covered from two sides with a thin CuBi layer (indicated in blue), connecting at the apex of the tip. When a charge current is applied through this layer, spins split due to the spin Hall effect and spin-polarizes the tip. By adjusting the direction of the current the polarization is switched.*

References

[1] A. Schmidt, K. Fujita, E. Kim, M. Lawler, H. Eisaki, S. Uchida, D. Lee, and J. Davis, *Electronic structure of the cuprate superconducting and pseudogap phases from spectroscopic imaging STM*, New Journal of Physics **13**, 065014 (2011).

[2] M. Allan, F. Massee, D. Morr, J. Van Dyke, A. Rost, A. Mackenzie, C. Petrovic, and J. Davis, *Imaging Cooper pairing of heavy fermions in CeCoIn5*, Nature Physics **9**, 468 (2013).

[3] T.-M. Chuang, M. Allan, J. Lee, Y. Xie, N. Ni, S. Bud'ko, G. Boebinger, P. Canfield, and J. Davis, *Nematic Electronic Structure in the "Parent" State of the Iron-Based Superconductor Ca (Fe1–xCox) 2As2*, Science **327**, 181 (2010).

[4] R. Wiesendanger, H.-J. Güntherodt, G. Güntherodt, R. Gambino, and R. Ruf, *Observation of vacuum tunneling of spin-polarized electrons with the scanning tunneling microscope*, Physical Review Letters **65**, 247 (1990).

[5] T. K. Yamada, M. Bischoff, T. Mizoguchi, and H. van Kempen, *Use of voltage pulses to detect spin-polarized tunneling*, Applied physics letters **82**, 1437 (2003).

[6] A. Kubetzka, M. Bode, O. Pietzsch, and R. Wiesendanger, *Spin-polarized scanning tunneling microscopy with antiferromagnetic probe tips*, Physical review letters **88**, 057201 (2002).

[7] T. Hanaguri, C. Lupien, Y. Kohsaka, D.-H. Lee, M. Azuma, M. Takano, H. Takagi, and J. Davis, *A 'checkerboard'electronic crystal state in lightly hole-doped Ca2-xNaxCuO2Cl2*, Nature **430**, 1001 (2004).

[8] M. D'yakonov and V. Perel, *Possibility of orienting electron spins with current*, Soviet Journal of Experimental and Theoretical Physics Letters **13**, 467 (1971).

[9] J. Hirsch, *Spin hall effect*, Physical Review Letters **83**, 1834 (1999).

[10] S. Zhang, *Spin Hall effect in the presence of spin diffusion*, Physical review letters **85**, 393 (2000).

[11] J. Sinova, D. Culcer, Q. Niu, N. Sinitsyn, T. Jungwirth, and A. MacDonald, *Universal intrinsic spin Hall effect*, Physical review letters **92**, 126603 (2004).

[12] J. Sinova, S. O. Valenzuela, J. Wunderlich, C. Back, and T. Jungwirth, *Spin Hall effect*, arXiv preprint arXiv:1411.3249 (2014).

[13] P. M. Levy, H. Yang, M. Chshiev, and A. Fert, *Spin Hall effect induced by Bi impurities in Cu: Skew scattering and side-jump*, Physical Review B **88**, 214432 (2013).

[14] J. Smit, *The spontaneous Hall effect in ferromagnetics II*, Physica **24**, 39 (1958).

[15] L. Berger, *Side-jump mechanism for the Hall effect of ferromagnets*, Physical Review B **2**, 4559 (1970).

[16] C. Herschbach, D. V. Fedorov, I. Mertig, M. Gradhand, K. Chadova, H. Ebert, and D. Ködderitzsch, *Insight into the skew-scattering mechanism of the spin Hall effect: Potential scattering versus spin-orbit scattering*, Physical Review B **88**, 205102 (2013).

[17] D. Culcer, E. Hankiewicz, G. Vignale, and R. Winkler, *Side jumps in the spin Hall effect: Construction of the Boltzmann collision integral*, Physical Review B **81**, 125332 (2010).

[18] S. O. Valenzuela and M. Tinkham, *Direct electronic measurement of the spin Hall effect*, Nature **442**, 176 (2006).

[19] T. Kimura, Y. Otani, T. Sato, S. Takahashi, and S. Maekawa, *Room-temperature reversible spin Hall effect*, Physical review letters **98**, 156601 (2007).

[20] L. Liu, C.-F. Pai, Y. Li, H. Tseng, D. Ralph, and R. Buhrman, *Spin-torque switching with the giant spin Hall effect of tantalum*, Science **336**, 555 (2012).

[21] C.-F. Pai, L. Liu, Y. Li, H. Tseng, D. Ralph, and R. Buhrman, *Spin transfer torque devices utilizing the giant spin Hall effect of tungsten*, Applied Physics Letters **101**, 122404 (2012).

[22] J. Bass and W. P. Pratt Jr, *Spin-diffusion lengths in metals and alloys, and spin-flipping at metal/metal interfaces: an experimentalist's critical review*, Journal of Physics: Condensed Matter **19**, 183201 (2007).

[23] M. Gradhand, D. V. Fedorov, P. Zahn, and I. Mertig, *Spin Hall angle versus spin diffusion length: Tailored by impurities*, Physical Review B **81**, 245109 (2010).

[24] A. Fert and P. M. Levy, *Spin Hall effect induced by resonant scattering on impurities in metals*, Physical review letters **106**, 157208 (2011).

[25] M. Gradhand, D. V. Fedorov, P. Zahn, and I. Mertig, *Extrinsic spin Hall effect from first principles*, Physical review letters **104**, 186403 (2010).

[26] Y. Niimi, M. Morota, D. Wei, C. Deranlot, M. Basletic, A. Hamzic, A. Fert, and Y. Otani, *Extrinsic spin Hall effect induced by iridium impurities in copper*, Physical review letters **106**, 126601 (2011).

[27] Y. Niimi, D. Wei, H. Idzuchi, T. Wakamura, T. Kato, and Y. Otani, *Experimental verification of comparability between spin-orbit and spin-diffusion lengths*, Physical review letters **110**, 016805 (2013).

[28] P. Laczkowski, J.-C. Rojas-Sánchez, W. Savero-Torres, H. Jaffrès, N. Reyren, C. Deranlot, L. Notin, C. Beigné, A. Marty, J.-P. Attané, L. Vila, J.-M. George, and A. Fert, *Experimental evidences of a large extrinsic spin Hall effect in AuW alloy*, Applied Physics Letters **104**, 142403 (2014).

[29] B. Gu, I. Sugai, T. Ziman, G. Guo, N. Nagaosa, T. Seki, K. Takanashi, and S. Maekawa, *Surface-assisted spin Hall effect in Au films with Pt impurities*, Physical review letters **105**, 216401 (2010).

[30] Y. Niimi, Y. Kawanishi, D. Wei, C. Deranlot, H. Yang, M. Chshiev, T. Valet, A. Fert, and Y. Otani, *Giant spin Hall effect induced by skew scattering from bismuth impurities inside thin film CuBi alloys*, Physical review letters **109**, 156602 (2012).

[31] Y. Niimi, H. Suzuki, Y. Kawanishi, Y. Omori, T. Valet, A. Fert, and Y. Otani, *Extrinsic spin Hall effects measured with lateral spin valve structures*, Physical Review B **89**, 054401 (2014).

[32] C. Herschbach, D. V. Fedorov, M. Gradhand, and I. Mertig, *Colossal spin Hall effect in ultrathin metallic films*, Physical Review B **90**, 180406 (2014).

[33] C. Brüne, A. Roth, E. Novik, M. König, H. Buhmann, E. Hankiewicz, W. Hanke, J. Sinova, and L. Molenkamp, *Evidence for the ballistic intrinsic spin Hall effect in HgTe nanostructures*, Nature Physics **6**, 448 (2010).

[34] D. Abanin, A. Shytov, L. Levitov, and B. Halperin, *Nonlocal charge transport mediated by spin diffusion in the spin Hall effect regime*, Physical review B **79**, 035304 (2009).

[35] L. Van der Pauw, *A method of measuring the resistivity and Hall coefficient on lamellae of arbitrary shape*, Philips technical review **20**, 220 (1958).

[36] A. Finkler, Y. Segev, Y. Myasoedov, M. L. Rappaport, L. Ne'eman, D. Vasyukov, E. Zeldov, M. E. Huber, J. Martin, and A. Yacoby, *Self-aligned nanoscale SQUID on a tip*, Nano letters **10**, 1046 (2010).

[37] A. Finkler, D. Vasyukov, Y. Segev, L. Ne'eman, E. Lachman, M. Rappaport, Y. Myasoedov, E. Zeldov, and M. Huber, *Scanning superconducting quantum interference device on a tip for magnetic imaging of nanoscale phenomena*, Review of Scientific Instruments **83**, 073702 (2012).

[38] D. Vasyukov, Y. Anahory, L. Embon, D. Halbertal, J. Cuppens, L. Neeman, A. Finkler, Y. Segev, Y. Myasoedov, M. L. Rappaport, M. E. Huber, and E. Zeldov, *A scanning superconducting quantum interference device with single electron spin sensitivity*, Nature nanotechnology **8**, 639 (2013).

[39] Y. Anahory, J. Reiner, L. Embon, D. Halbertal, A. Yakovenko, Y. Myasoedov, M. L. Rappaport, M. E. Huber, and E. Zeldov, *Three-Junction SQUID-on-Tip with Tunable In-Plane and Out-of-Plane Magnetic Field Sensitivity*, Nano letters **14**, 6481 (2014).